MCB
Journals.ASM.org

BNip3 Regulates Mitochondrial Function and Lipid Metabolism in the Liver

Danielle Glick,[a,b] Wenshuo Zhang,[c,d] Michelle Beaton,[a,c] Glenn Marsboom,[d] Michaela Gruber,[e] M. Celeste Simon,[e] John Hart,[f] Gerald W. Dorn II,[g] Matthew J. Brady,[c,d] and Kay F. Macleod[a,b,c]

Ben May Department for Cancer Research, The Gordon Center for Integrative Sciences, The University of Chicago, Chicago Illinois, USA[a]; Committee on Cancer Biology, The University of Chicago, Chicago, Illinois, USA[b]; Committee on Molecular Metabolism & Nutrition, The University of Chicago, Chicago, Illinois, USA[c]; Department of Medicine, The University of Chicago, Chicago, Illinois, USA[d]; Abramson Family Cancer Research Institute, University of Pennsylvania Medical School, Philadelphia, Pennsylvania, USA[e]; Department of Pathology, The University of Chicago, Chicago, Illinois, USA[f]; and Department of Internal Medicine, Washington University School of Medicine, St. Louis, Missouri, USA[g]

BNip3 localizes to the outer mitochondrial membrane, where it functions in mitophagy and mitochondrial dynamics. While the BNip3 protein is constitutively expressed in adult liver from fed mice, we have shown that its expression is superinduced by fasting of mice, consistent with a role in responses to nutrient deprivation. Loss of BNip3 resulted in increased lipid synthesis in the liver that was associated with elevated ATP levels, reduced AMP-regulated kinase (AMPK) activity, and increased expression of lipogenic enzymes. Conversely, there was reduced β-oxidation of fatty acids in BNip3 null liver and also defective glucose output under fasting conditions. These metabolic defects in BNip3 null liver were linked to increased mitochondrial mass and increased hepatocellular respiration in the presence of glucose. However, despite elevated mitochondrial mass, an increased proportion of mitochondria exhibited loss of mitochondrial membrane potential, abnormal structure, and reduced oxygen consumption. Elevated reactive oxygen species, inflammation, and features of steatohepatitis were also observed in the livers of BNip3 null mice. These results identify a role for BNip3 in limiting mitochondrial mass and maintaining mitochondrial integrity in the liver that has consequences for lipid metabolism and disease.

Modulation of mitochondrial mass is emerging as a major adaptive response to changes in energy balance arising from deficiencies in oxygen or glucose availability, among other nutrient stresses. For example, nutrient-sensitive changes in PGC-1α activity alter expression of genes required for mitochondrial biogenesis, in addition to genes required for fatty acid metabolism (17, 38). While mitochondrial biogenesis increases mitochondrial mass, this is countered by the role of mitophagy in targeting dysfunctional mitochondria for degradation at the autophagosome, resulting in reduced mitochondrial mass (28, 29, 70). Defects in autophagy have been linked to liver cancer (25, 44, 65) and have also been shown to promote hepatic insulin resistance (19, 67). However, this cannot be attributed to defective mitochondrial function, since autophagy-deficient liver also exhibits increased endoplasmic reticulum (ER) stress (67), protein aggregation (31), and defective lipidophagy (59). To date, a specific role for mitophagy in preventing hepatic steatosis or other liver pathologies has not been identified.

Hypoxia modulates mitochondrial mass through both decreasing mitochondrial biogenesis (74) and increasing mitophagy (3, 64, 73). These effects are mediated by hypoxia-inducible factor (HIF) transcription factors, acting on the one hand to inhibit Myc-induced expression of PGC-1β (74) and on the other to induce expression of the mitochondrial proteins BNIP3 and NIX (3, 4, 64, 73). Initial functional characterization of BNIP3 and NIX indicated that these proteins were loosely conserved members of the BH3-only subgroup of the Bcl-2 family of cell death regulators (7, 8, 52, 68), and indeed, evidence from ischemia-reperfusion injury experiments in cardiomyocytes supports a prodeath function for both BNip3 and Nix (15, 22, 60), although this likely requires a second signal, such as acidosis or calcium release from the endoplasmic reticulum (9, 16, 34, 75).

A role for BNIP3 and NIX in promoting cell death in response to specific stresses has been offset by evidence that overexpression of BNIP3 is not sufficient to kill cells (49, 64) but rather promotes mitochondrial fragmentation and mitophagy through interactions with OPA-1 and LC-3, respectively (35, 53). Similarly, NIX plays a key role in the maturation of red blood cells through developmentally regulated induction of mitophagy (55, 57) that involves interactions with the LC3-related molecule GABARAP (56). Thus, BNIP3 and NIX appear to play dual roles in both mitophagy and cell death, although how the cell switches between these different functions is not clear.

In the present study, we found that BNip3 is expressed at markedly higher levels in adult mouse liver than in most other tissues examined and was further induced to very high levels in liver by overnight fasting. Given the importance of mitochondrial function in metabolism and evidence that hypoxia regulates both mitophagy and metabolic processes (32, 42, 51), we were thus interested in examining the consequences of BNip3 loss for cellular and systemic metabolism. We have shown for the first time that BNip3 is required to prevent excess lipid accumulation in the liver and to promote hepatic glucose output in response to fasting and that loss of BNip3 leads to steatohepatitis. These defects were linked to both increased mitochondrial mass and increased mitochondrial

Received 6 February 2012 **Returned for modification** 25 March 2012
Accepted 24 April 2012
Published ahead of print 30 April 2012
Address correspondence to Kay F. Macleod, kmacleod@uchicago.edu

doi:10.1128/MCB.00167-12

dysfunction, demonstrating the importance of proper control of mitophagy for normal liver metabolism and for prevention of liver disease.

MATERIALS AND METHODS

Mice. Wild-type, BNip3 heterozygous, and BNip3 null mice were maintained on a pure C57B/6 genetic background. Male mice were used for all analyses and were generally used with age-matched control littermates between the ages of 3 and 5 months of age unless otherwise stated. Mice were fasted for 24 h for experiments unless stated otherwise. All mice were housed in a barrier facility, fed normal chow, and kept on a 12-h-light/12-h-dark cycle. Conditionally targeted Hif-1$\alpha^{\Delta/\Delta}$, Hif-2$\alpha^{\Delta/\Delta}$, and Arnt$^{\Delta/\Delta}$ mice were generated as reported previously (20).

***In vivo* metabolic assays and measurements.** Three- to five-month-old male mice were fasted for 16 h for a glucose tolerance test (GTT), glucagon stimulation test (GST), pyruvate challenge (PC), or alanine challenge (AC), while a 4-h fast was used for the insulin tolerance tests (ITT). The GTT was performed by intraperitoneal (i.p.) injection of 2 g D-glucose/kg body weight, ITT was conducted using 20 U insulin/kg, PC was done by injection of 1.5 g/kg sodium pyruvate, AC was carried out by injection of 1.0 g/kg alanine, and GST was conducted using 20 mg/kg of glucagon (Sigma). Glucose measurements were made using a Freestyle Lite glucometer, and serum insulin was measured by enzyme-linked immunosorbent assay (ELISA) (Alpco).

Primary hepatocyte culture, *in vitro* assays, and cell staining. Primary hepatocytes were obtained by collagenase perfusion of live mice as described previously (71) with the following modifications: type IV collagenase (100 U/ml; Worthington Biochemical) was used for digestion, the flow rate was 9 ml/min, medium used for isolation and plating was Dulbecco's modified Eagle medium (DMEM) with 25 mM glucose and 10% fetal bovine serum (FBS), and viability as determined by trypan blue staining was >90% for all preparations. Cells were plated on collagen-coated (8 $\mu g/cm^2$) plates. Cells were maintained overnight in serum-free DMEM containing 5 to 25 mM glucose, and all cells were used within 30 h of plating. Total intracellular glycogen was assessed by a modification of the methods outlined in reference 39. Gluconeogenesis was evaluated by measurement of glucose released into the medium via the 2,2′-azinobis(3-ethylbenzthiazolinesulfonic acid (ABTS)-linked glucose oxidase-peroxidase method. Medium was changed to glucose-free phenol red-free DMEM (Mediatech) containing 10 mM lactate or glycerol; forskolin (25 μM), if used, was added at the start of the assay. Beta oxidation of [9,10-^{3}H]-palmitic acid (Perkin Elmer) was assessed based upon a modification of the method outlined previously (45). Sodium palmitate (200 μM) was coupled to bovine serum albumin (BSA) in a 3-to-1 molar ratio. Carnitine (1 mM) was added at the start of the assay, while etomoxir (10 μM) was preincubated for 30 min prior to the start of the assay. Lipogenesis from glucose was determined by measuring the incorporation of [U-^{14}C]glucose (American Radiolabeled Chemicals) into the lipid-extractable fraction of cell lysates. Cells were lysed in H_2O, scraped into scintillation vials containing organic scintillation fluid (Betafluor; National Diagnostics), and vigorously shaken. Radioactivity in the organic fraction was quantified using a scintillation counter. Fluorescence microscopy of live or methanol-fixed primary hepatocytes was performed using boron-dipyrromethene (BODIPY) (Invitrogen), 1 mM tetramethylrhodamine, ethyl ester (TMRE) (Invitrogen), and anti-heat shock protein 60 (anti-HSP60) antibodies (Stressgen) and analyzed on Zeiss Axiovert 200 M microscope.

Western blot analyses. Snap-frozen tissues were pulverized and extracted in an equal volume of either RIPA extraction buffer (1% sodium deoxycholate, 0.1% SDS, 1% Triton X-100, 10 mM Tris-HCl, pH 8.0, and 0.14 M NaCl) or NP-40 lysis buffer (150 mM NaCl, 50 mM Tris-HCl, pH 7.5, 0.5% NP-40, and 5 mM β-mercaptoethanol) for Western blotting. Primary antibodies to BNip3 (Sigma, Cell Signaling), Acly, malic enzyme, α-tubulin (all from Abcam), Cox IV (Mitosciences), HSP60, cytochrome *c*, AMP-regulated kinase (AMPK), phosphorylated AMPK (p-AMPK), Acc, Fasn, Raptor, p-Raptor (all Cell Signaling), and LC-3B (Novus) were used with appropriate secondary antibodies prior to detection carried out by enhanced chemiluminescence (ECL film; GE Healthcare). All blots were performed at least three times.

Transmission electron microscopy. Small pieces of liver were fixed in 2.5% gluteraldehyde, and sections were analyzed using a Philips CM120 transmission electron microscope.

Quantitative PCR. Total genomic DNA was isolated from adult liver using standard approaches. Relative mitochondrial-to-nuclear genome ratios were determined using TaqMan real-time PCR primers specific to mitochondrial genome-encoded NADH dehydrogenase subunit 1 (*Nd1*) and cytochrome *b* (*cytb*) and to nuclear genome encoded β-globin. Total RNA was extracted from whole liver using TRIzol reagent (Invitrogen). cDNA synthesis from total RNA was performed using the High Capacity RNA-to-cDNA master mix (Applied Biosystems). mRNA levels were quantified by real-time PCR using TaqMan primers, and all samples were analyzed in triplicate. Relative quantification of RNA amounts was determined using the comparative threshold cycle (C_T) method. Relative amounts of mRNA for genes analyzed were normalized to endogenous control β-actin and expressed relative to wild-type amounts (reference sample). Relative levels of mouse FBP1, Pepck, and Pklr were determined using specific TaqMan real-time PCR primers.

Immunohistochemistry and tissue staining. Tissues were frozen in O.C.T. compound (TissueTEK) for sectioning and staining for oil red O or dihydroethidine (catalog no. D23107; Sigma). Alternatively, tissues were fixed in 10% neutral buffered formalin embedded in paraffin, and sections were stained with periodic acid-Schiff (PAS) stain, terminal deoxynucleotidyltransferase-mediated dUTP-biotin nick end labeling (TUNEL), and other immunohistochemical stains, using citrate buffer and heat denaturation of the epitope, as described previously (41). Liver sections were incubated in biotin block prior to addition of primary antibody, developed using Envision System horseradish peroxidase (HRP) (Dako), and counterstained in hematoxylin.

Measurements of NADPH and ATP. A commercially available colorimetric assay kit (catalog number 65349; Abcam) was used to measure levels of NADPH in fresh liver. ATP/ADP ratios were determined by measuring total ATP with an ATP bioluminescence assay kit, CLS II (catalog number 11 699 695 001; Roche) before and after conversion of ADP to ATP.

Measurements of OCR. A Seahorse Bioscience instrument (model XF24) was used to measure the rate of change in dissolved O_2 in either: (i) DMEM buffered to pH 6.8 with piperazine-*N*,*N*′-bis(2-ethanesulfonic acid) (PIPES) for whole hepatocytes or (ii) mitochondrial assay medium (70 mM sucrose, 220 mM mannitol, 10 mM KH_2PO_4, 5 mM $MgCl_2$, 2 mM HEPES, 1 mM EGTA, 0.2% fat-free BSA) for mitochondria isolated from primary hepatocytes, both in custom 24-well plates. Confluent hepatocyte cultures were plated overnight, and the oxygen consumption rate (OCR) was measured the next day in 2 μM oligomycin (port A), 1 μM FCCP (port B), and 1 μM antimycin A (port C). The OCR for whole hepatocytes was then standardized for total protein concentration after the assay was completed. For isolated mitochondrial OCR measurements, 40 μg of isolated mitochondria in 50 μl were centrifuged to the bottom of each well of a 24-well plate in the presence of 10 mM pyruvate-malate or 80 μM palmitoyl-carnitine–0.5 mM malate and incubated for 10 min at 37°C. Mitochondrial oxygen consumption was determined in 4 mM ADP (port A), 2.5 μg/ml oligomycin (port B), 4 μM carbonyl cyanide *p*-(trifluoromethoxy)phenylhydrazon (FCCP) (port C), and 4 μM antimycin A (port D). Measurements of O_2 concentration were reported in pmol/min at each time point.

Metabolomic analysis. Unbiased analysis of levels of acyl carnitines in wild-type and BNip3 null livers, fed and fasted, was performed by liquid chromatography-mass spectrometry (LC-MS) by the University of Michigan Nutrition Obesity Research Center (UMNORC), which is supported by grant DK089503 from the NIH to the University of Michigan.

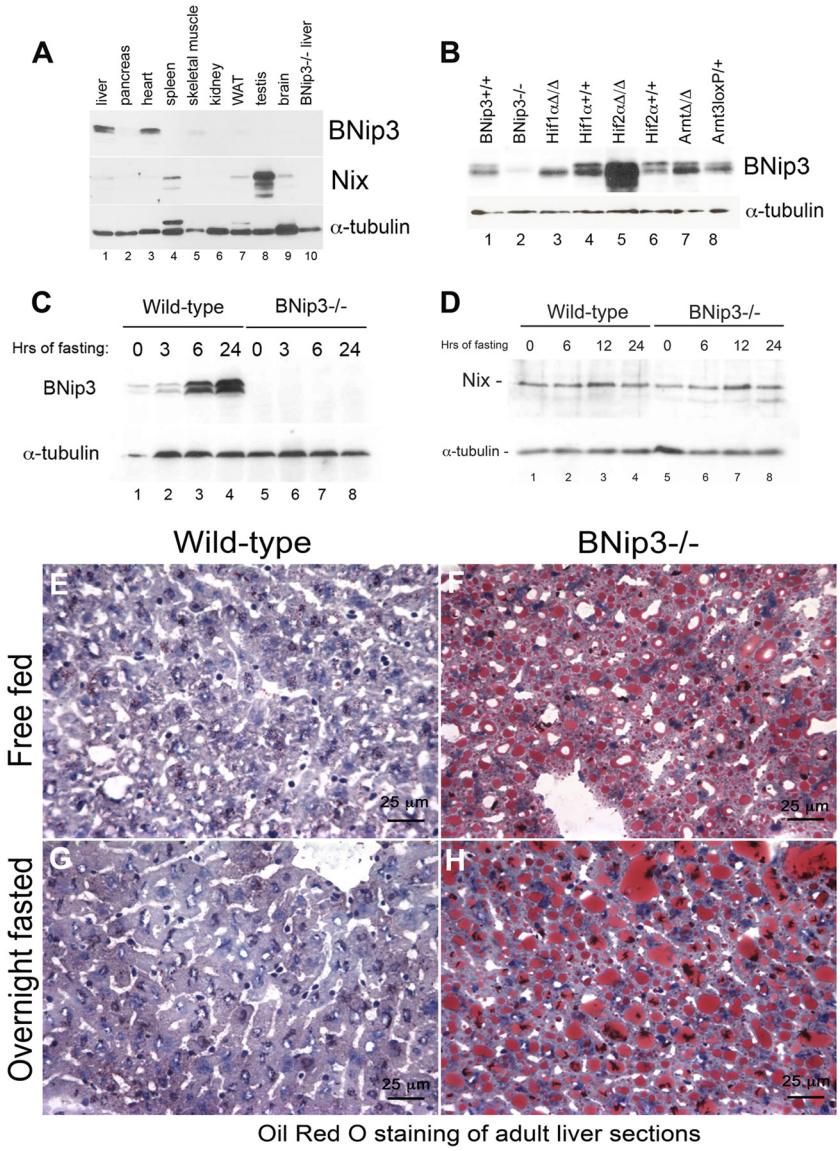

FIG 1 (A) Western blot for BNip3 and Nix (and α-tubulin as a loading control) on whole-cell extracts from adult mouse tissues (liver, pancreas, heart, spleen, skeletal muscle, kidney, white adipose tissue [WAT], testis, and brain). (B) Western blot for BNip3 on whole-cell lysates extracted from wild-type, BNip3 null, Hif-1α-deleted, Hif-1α control, Hif-2α-deleted, Hif-2α control, Arnt-deleted, or Arnt control livers. (C) Western blot for BNip3 on whole-cell liver extracts from wild-type and BNip3 null mice that were fasted for 0, 3, 6, or 24 h. (D) Western blot for Nix on whole-cell liver extracts from wild-type and BNip3 null mice that were fasted for 0, 6, 12, or 24 h. (E to H) Oil red O staining of frozen liver sections from wild-type (E and G) or BNip3 null (F and H) mice that were either free fed (E and F) or fasted (G and H) for 24 h.

RESULTS

BNip3 is expressed in healthy adult liver. When we examined expression of both the BNip3 and Nix proteins in adult mouse tissues by Western blotting (Fig. 1A), we observed high-level expression of BNip3 in the liver and the heart (Fig. 1A, lanes 1 and 3, respectively), very low expression in skeletal muscle (Fig. 1A, lane 5), and undetectable BNip3 expression in other tissues examined (Fig. 1A, lanes 2, 4, and 6 to 9). Nix was expressed at higher levels in the spleen and testis (Fig. 1A, lanes 4 and 8) than in other tissues but was not readily detectable in the liver (Fig. 1A, lane 1). Elevated expression of Nix in the spleen is consistent with a role for Nix in end-stage red blood cells that are present in the red pulp of adult spleen (55, 57), while high level BNip3 expression in the heart supports an important role for BNip3 in mitochondrial function in cardiomyocytes (18). Interestingly, Western blotting for BNip3 on extracts from liver derived from mice carrying induced deletion of Hif-1α, Hif-2α, or Arnt/Hif-1β showed that expression of BNip3 in the liver was not dependent on Hif activity, since it was still expressed in Arnt-deleted liver (Fig. 1B, lane 7). However, BNip3 was substantially induced in the liver of mice with induced deletion of Hif-2α (Fig. 1B, lane 5), suggesting that BNip3 is directly or indirectly repressed by Hif-2α in adult mouse liver. Robust expression of BNip3 in healthy adult liver is not consistent with a cell death function for BNip3 in this tissue, and since a role for BNip3 in normal liver had not been previously reported, we focused our experiments on defining this activity of BNip3.

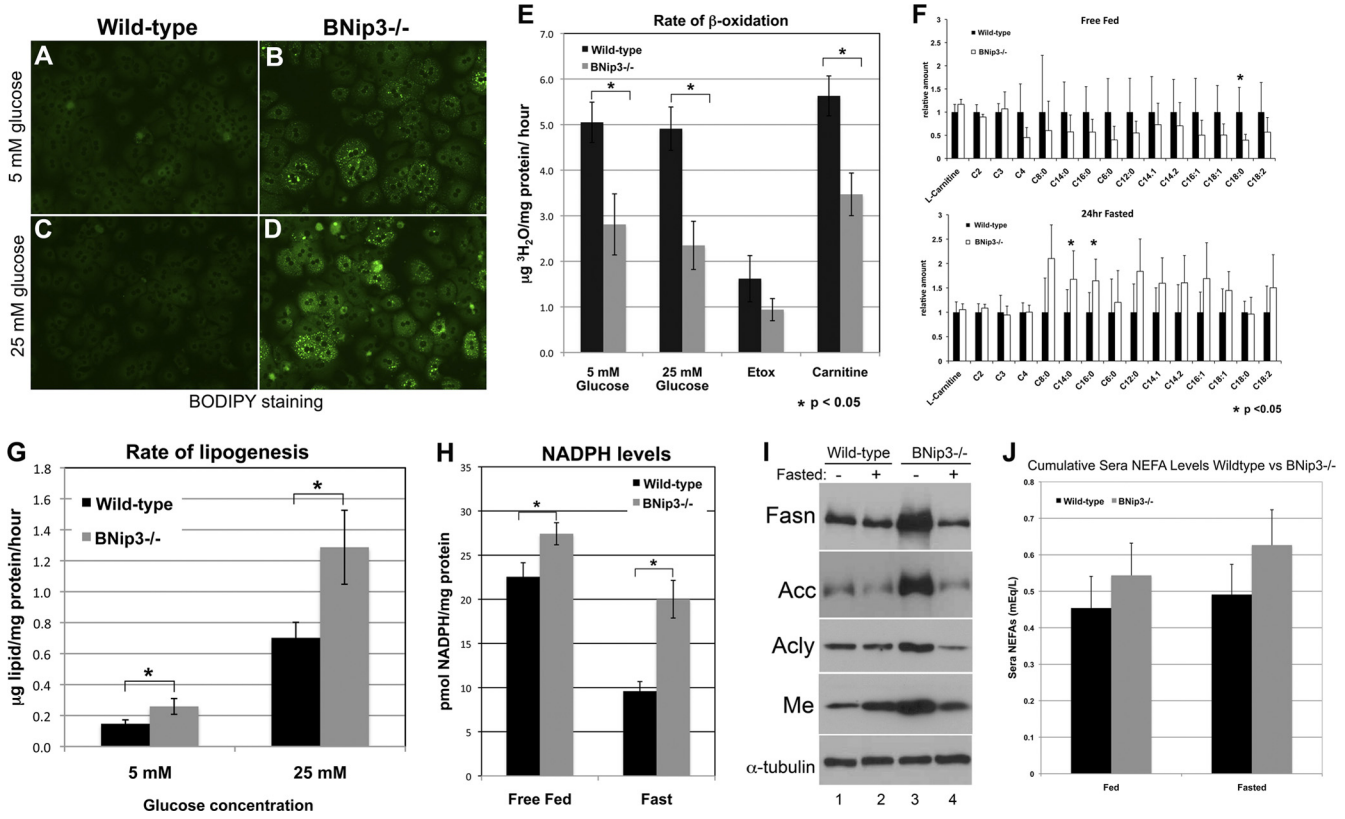

FIG 2 (A to D) Fluorescence microscopy of wild-type and BNip3 null hepatocytes that were stained with the lipophilic dye BODIPY after growth in culture for 24 h in the presence of 5 mM (A and B) or 25 mM (C and D) glucose. (E) Conversion of tritiated palmitate to tritiated water in wild-type and BNip3 null hepatocytes as a proportion of total protein, in the presence of 5 mM glucose, 25 mM glucose, 10 μM etomoxir, or 1 mM carnitine ($n = 6$ for each treatment per genotype). (F) Mass spectrometric analysis of acyl carnitine levels (pmol/mg tissue) in wild-type and BNip3 null livers from free-fed or fasted mice. (G) Measurement of lipid formed in culture per hour in the presence of ^{13}C-labeled glucose at either a 5 mM ($n = 13$) or 25 mM ($n = 14$) concentration as a proportion of total protein for both wild-type and BNip3 null hepatocytes. The significance of differences in lipid synthesized between wild-type and Bnip3 null hepatocytes had a P value of 0.0529 at 5 mM and 0.0373 at 25 mM. (H) Measurement of total cytosolic NADPH as a proportion of total protein ($n = 6$ for each treatment per genotype). The significance of differences in NADPH levels between wild-type and Bnip3 null hepatocytes had a P value of 0.0714 under free-fed conditions and 0.0018 under fasted conditions. (I) Western blot analysis for fatty acid synthase (Fasn), acetyl CoA-carboxylase 1/2 (Acc), ATP citrate lyase (Acly), malic enzyme (Me), and α-tubulin on whole-cell liver extracts from adult mice that are free fed (lanes 1 and 3) or fasted (lanes 2 and 4). (J) Measurement of serum nonesterified fatty acids (NEFA) in wild-type and BNip3 null mice before and after 24 h of fasting. Data are represented as means + SEM. An unpaired Student t test was used for evaluation of statistical significance. The asterisk indicates $P < 0.05$.

BNip3 is induced in the liver by fasting, while loss of BNip3 results in hepatic steatosis. Given the importance of the liver in systemic metabolism and responses to nutrient deprivation (38, 46, 54), we examined expression of BNip3 in the liver of fasted mice. The BNip3 protein was markedly induced above basal levels by 6 h of fasting, with further induction by 24 h of fasting (Fig. 1C). In contrast, we did not observe any induction of Nix in the liver of fasted mice (Fig. 1D). Oil red O staining of liver sections from free-fed mice showed that BNip3 null liver (Fig. 1F) was markedly more steatotic than the wild type (Fig. 1E) under normal dietary conditions. Fasting of mice promotes lipid mobilization from adipocytes into the liver for oxidation, and overnight fasting of BNip3 null mice showed further lipid accumulation, with larger, more numerous lipid vesicles apparent in oil red O-stained liver sections (Fig. 1H) than was observed for fasted wild-type mice (Fig. 1G). These results show for the first time that BNip3 protein levels in the liver are regulated in response to nutrient availability and that loss of BNip3 results in hepatic steatosis.

Increased lipogenesis and reduced β-oxidation of fatty acids in BNip3 null liver. To investigate the cause of hepatic steatosis in BNip3 null mice, we examined lipid accumulation, as well as the rates of both fatty acid oxidation and lipid synthesis, in cultured primary hepatocytes from wild-type and BNip3 null livers. Staining of primary hepatocytes from wild-type and BNip3 null liver with BODIPY (a lipophilic dye) showed that BNip3 null hepatocytes stained more strongly for BODIPY (Fig. 2B) than wild-type hepatocytes (Fig. 2A) when grown overnight in 5 mM glucose (a physiologically relevant concentration), consistent with greater lipid accumulation in BNip3 null hepatocytes than for the wild type. This indicated that BNip3 null hepatocytes *in vitro* recapitulated the steatotic phenotype observed *in vivo* (Fig. 1). The amount of lipid accumulation increased in proportion to the amount of glucose in the culture medium, with increased BODIPY staining of BNip3 null hepatocytes at 25 mM glucose (Fig. 2D) compared to that at 5 mM (Fig. 2B).

Increased lipid accumulation can be attributed to either reduced β-oxidation of fatty acids or increased lipid synthesis. When we measured the rate of fatty acid oxidation in cultured hepatocytes in the presence of 5 mM or 25 mM glucose, we observed a 2- to 3-fold decrease in the β-oxidation of fatty acids in

BNip3 null liver compared to that in wild-type liver (Fig. 2E). The efficiency of β-oxidation was increased to a greater extent in BNip3 null hepatocytes than in wild-type hepatocytes by treatment with 1 mM carnitine, which promotes fatty acid uptake by mitochondria, consistent with reduced fatty acid import into BNip3 null mitochondria. However, β-oxidation remained lower in BNip3 null hepatocytes than in wild-type ones, arguing that reduced carnitine availability was not sufficient to explain the full extent of reduced β-oxidation of fatty acids in BNip3 null liver (Fig. 2E). Consistently, oxidation of fatty acids in BNip3 null hepatocytes was inhibited to a similar extent as that for the wild type by treatment with 10 μM etomoxir, an inhibitor of carnitine palmitate transporter 1 (Cpt-1) (Fig. 2E), indicating that while fatty acid transport into the mitochondria of BNip3 null hepatocytes was reduced, it was not completely defective.

Supporting these *in vitro* findings, metabolomic analysis of acyl carnitine content in BNip3 null liver demonstrated a marked reduction in mitochondrial content of acyl carnitines under fed conditions compared to results for liver from wild-type mice, suggesting reduced import of fatty acids into the mitochondria in BNip3 null hepatocytes in the fed state (Fig. 2F). In contrast, increased long-chain acyl carnitines (C_{14} and C_{16} in particular) showed increased concentrations in fasted BNip3 null liver compared to those in wild-type liver, consistent with reduced β-oxidation of fatty acids in BNip3 null mitochondria under fasting conditions (Fig. 2F). These results suggest that there is increased lipid content in BNip3 null liver under fed and fasted conditions, at least in part due to reduced β-oxidation of fatty acids in BNip3 null liver (Fig. 1F).

Increased lipid content could also be explained by an increased rate of *de novo* lipid synthesis, and indeed, we observed a 2-fold increase in the rate of conversion of glucose to lipid in BNip3 null hepatocytes compared to that for the wild type when grown in 5 mM glucose *in vitro* (Fig. 2G). Consistent with BODIPY staining, lipid synthesis increased further in BNip3 null hepatocytes when the concentration of glucose in the medium was increased to 25 mM, such that now we observed a 3- to 4-fold increase in lipid synthesis over that for the wild type (Fig. 2G). Lipid synthesis requires the reducing power of NADPH, generated in the cytosol through the pentose phosphate pathway or the pyruvate-malate cycle. Consistent with elevated *de novo* lipid synthesis in BNip3 null primary hepatocytes *in vitro*, we detected elevated cytosolic NADPH levels *in vivo* in BNip3 null liver from both fed and fasted mice compared to wild-type levels (Fig. 2H). Furthermore, the decrease in cytosolic NADPH upon fasting was significantly smaller in the BNip3 null liver (1.37-fold) than in wild-type liver (2.45-fold) (Fig. 2H). We also detected elevated expression of the key enzymes, fatty acid synthase (Fasn), acetyl-coenzyme A (CoA) carboxylase (Acc), and ATP citrate lyase (Acly), as well as malic enzyme (Me), in BNip3 null liver from free-fed mice compared to that in wild-type livers (Fig. 2I, lane 3). Acly, Acc, and Fasn are all enzymes involved in lipid biosynthesis from cytosolic citrate, and their upregulation (Fig. 2I, lane 3), alongside increased NADPH (Fig. 2H), is consistent with increased lipid synthesis in BNip3 null liver (Fig. 1F), while increased expression of malic enzyme, which catalyzes the conversion of malate to pyruvate, likely contributes to increased NADPH levels (Fig. 2H). Interestingly, increased expression of Acc in BNip3 null liver under fed conditions (Fig. 2I, lane 3) may also explain reduced import of fatty acids into the mitochondria, which contributes to reduced fatty acid oxidation (Fig. 2E). Increased lipid synthesis and increased levels of lipogenic enzymes suggested that loss of BNip3 resulted in the aberrant sensing of a high-energy state in the livers of free-fed mice. Fasting is expected to reduce this high-energy state, and consistently, we observed reduced expression of lipogenic enzymes in BNip3 null liver from fasted mice (Fig. 2I, lane 4). Thus, BNip3 null hepatocytes are able to receive and respond to the fasting signal but are nevertheless unable to reverse lipid accumulation, possibly due to the continued defect in β-oxidation of fatty acids in BNip3 null hepatocytes (Fig. 2E and F). In summary, we observed that loss of BNip3 leads to reduced β-oxidation of fatty acids and increased *de novo* lipogenesis in cultured hepatocytes and that this is associated with deregulated transport and oxidation of acyl carnitines, liver steatosis, increased NADPH, and increased expression of lipogenic enzymes *in vivo*.

Elevated lipid in the liver was not accompanied by a significant increase in serum free fatty acids (Fig. 2J). Nor was increased liver steatosis associated with an increase in overall body mass, increased fat-mass-to-lean-mass ratio, or increased food consumption in BNip3 null mice compared to results for age-matched wild-type littermate control mice, and the respiratory exchange ratio for these mice was similar to age- and sex-matched wild-type mice under both fed and fasted conditions (data not shown). These observations suggest that hepatic steatosis in BNip3 null liver was not due to a systemic problem in metabolism but reflects a key function(s) for BNip3 in the liver.

Reduced hepatic glucose output in response to fasting in BNip3 null mice. Given the observed effects on hepatic lipid metabolism and the inextricable connection between lipid and glucose homeostasis in the liver, we next examined whether loss of BNip3 also affected glucose metabolism. We measured serum glucose levels in free fed and fasted mice and observed, as expected, a decrease in serum glucose in both wild-type and BNip3 null mice in response to fasting (Fig. 3A). However, the decrease in serum glucose was greater in fasted BNip3 null mice, suggesting a reduced capacity to increase the hepatic glucose output in response to fasting. The failure of fasted BNip3 null mice to maintain serum glucose levels compared to fasted wild-type mice was not associated with significant differences in serum insulin levels, which dropped to comparably low levels in both wild-type and BNip3 null mice in response to fasting (Fig. 3B). When BNip3 null mice were fasted overnight and then injected with 2.0 g/kg glucose, serum glucose levels remained at significantly lower levels than those in wild-type control mice (Fig. 3C). Again, this could not be attributed to significant differences in serum insulin levels between wild-type and BNip3 null mice during the glucose tolerance test (Fig. 3D). When BNip3 null mice were injected with 20 U/kg insulin, serum glucose levels also dropped much more significantly than in wild-type mice (Fig. 3E), such that BNip3 null mice challenged with insulin frequently became severely hypoglycemic and had to be injected with glucose to restore blood sugar levels. The increased insulin sensitivity observed in BNip3 null mice was matched by a marked reduction in the glucagon response. When stimulated with 20 μg/kg glucagon, BNip3 null mice showed a significantly lower rate of glucose export to the blood than wild-type mice stimulated with glucagon (Fig. 3F). These results indicate that in addition to defects in lipid metabolism, BNip3 null liver is defective in its ability to increase glucose output in response to fasting.

Defective gluconeogenesis in BNip3 null liver. In the imme-

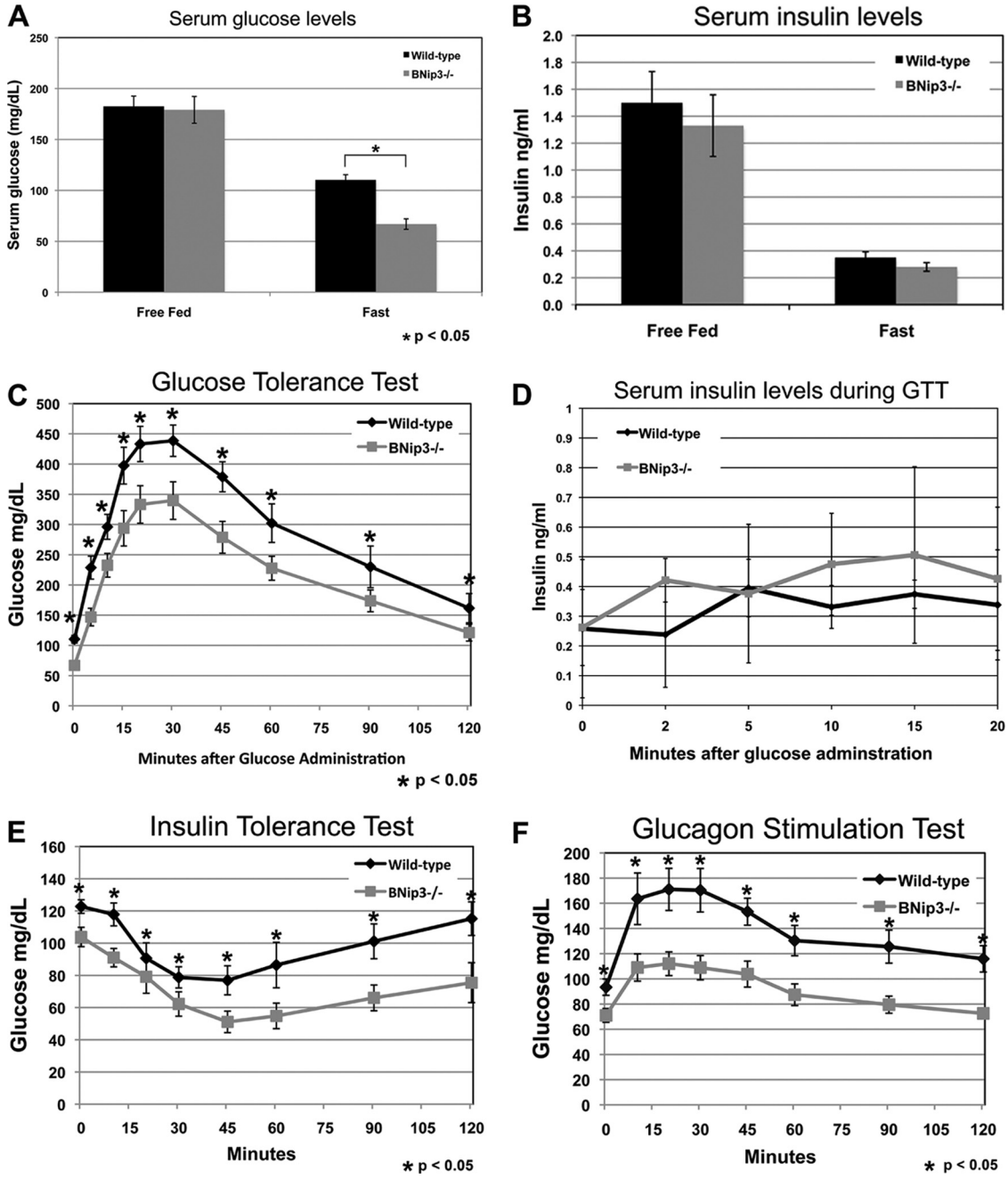

FIG 3 (A) Measurement of serum glucose in wild-type and BNip3 null mice before and after 24 h of fasting ($n = 9$ for free fed; $n = 14$ for fasted). Differences between wild-type and BNip3 null mice were insignificant under fed conditions. Under fasted conditions, the differences were significant ($P < 0.00002$). (B) Measurement of serum insulin in wild-type and BNip3 null mice before and after 24 h of fasting ($n = 17$ for free fed; $n = 13$ for fasted). Differences were not significant. (C) Glucose tolerance test measuring serum glucose in fasted mice at 15-min intervals after injection with 2 g/kg glucose ($n = 10$ for wild-type; $n = 14$ for BNip3 null). (D) Measurement of serum insulin in wild-type and BNip3 null mice during the GTT shown in panel C. (E) Insulin tolerance test measuring serum glucose in fasted mice at 15-min intervals after injection with 0.5 U/kg insulin ($n = 12$ for wild type; $n = 9$ for BNip3 null). (F) Glucagon sensitivity test measuring serum glucose in fasted mice at 15-min intervals after injection with 20 mg/kg glucagon ($n = 8$ for wild type; $n = 9$ for BNip3 null). Data are represented as means + SEM. An unpaired Student *t* test was used for evaluation of statistical significance. The asterisk indicates $P < 0.05$.

diate response to fasting, the liver mobilizes glycogen stores to supply energy to extrahepatic tissues in the form of glucose (38). The significant reduction in blood glucose levels post-24 h of fasting in BNip3 null mice (Fig. 3A) suggests that the defect in glucose export is not the result of a failure to store or mobilize glycogen, since glycogen breakdown is required during only the first few hours of fasting. Indeed, *in situ* staining with PAS showed a significant reduction in glycogen levels as expected in both the wild-type and BNip3 null livers following overnight fasting (Fig. 4A to D), consistent with effective sensing of the fasting signal in BNip3 null liver. Nevertheless, quantification of glycogen levels in the BNip3 null liver indicated that absolute levels of glycogen were

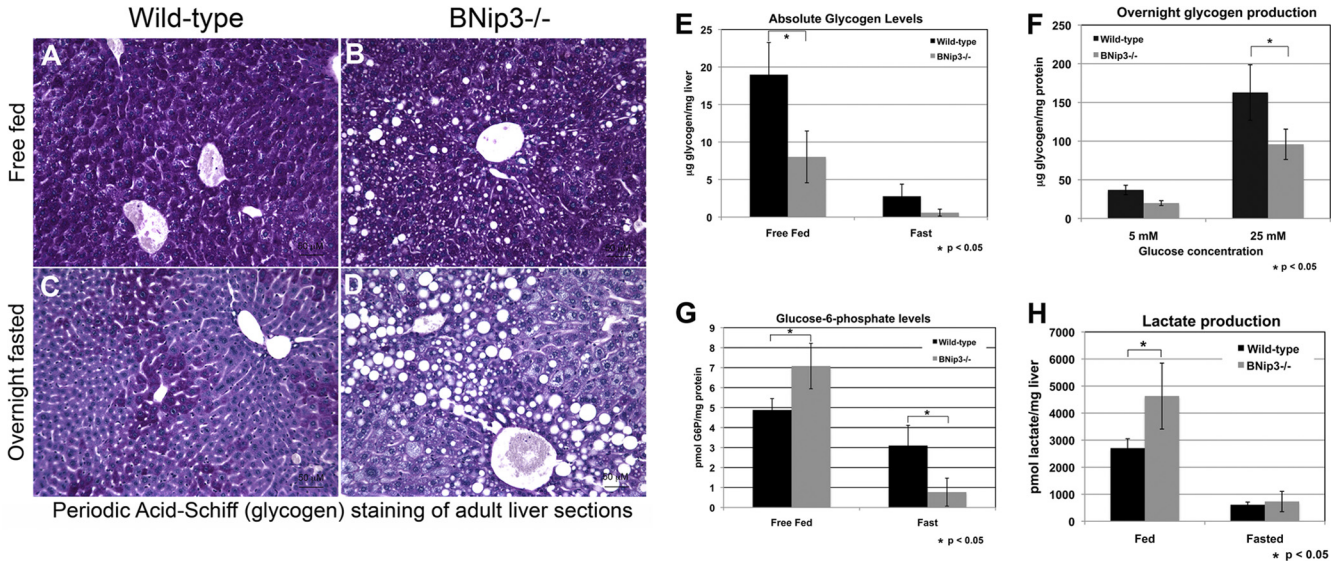

FIG 4 (A to D) *In situ* staining for hepatic glycogen using PAS stain on wild-type (A and C) or BNip3 null (B and D) livers from free-fed (A and B) or fasted (C and D) mice. (E) Measurement of absolute glycogen in livers from wild-type and BNip3 null mice that are free fed or fasted for 24 h ($n = 7$, wild type; $n = 6$, BNip3 null). (F) Rate of glycogen production by wild-type or BNip3 null hepatocytes grown overnight in culture medium containing either 5 mM or 25 mM glucose ($n = 10$ for all data sets). (G) Measurement of total cytosolic glucose-6-phosphate as a proportion of total protein for wild-type and BNip3 null livers ($n = 6$ for each data set). (H) LC-MS analysis of lactate levels as a proportion of total protein for wild-type and BNip3 null livers ($n = 4$ for each data set). Data are represented as means + SEM. An unpaired Student *t* test was used for evaluation of statistical significance. The asterisk indicates $P < 0.05$.

lower in BNip3 null liver than in the wild type, both in free-fed mice and in response to overnight fasting (Fig. 4E). Furthermore, BNip3 null hepatocytes accumulated less glycogen when cultured overnight in glucose (Fig. 4F). These observations showed that while BNip3 null liver is able to store glycogen under fed conditions and mobilize it in response to fasting, the overall levels were reduced under both sets of conditions. Reduced glycogen storage suggested that glycolysis might be increased. To examine this, we measured the levels of both glucose-6-phosphate and lactate in BNip3 null liver extracts compared to wild-type levels, again under fed and fasted conditions. We observed increased levels of both glucose-6-phosphate (Fig. 4G) and lactate (Fig. 4H) in BNip3 null liver compared to wild-type levels under fed conditions, consistent with increased glycolysis in BNip3 null liver. The levels of both of these glycolytic intermediates dropped significantly, as expected in response to reduced glucose uptake by the liver under fasted conditions.

Once liver glycogen stores are depleted within the first few hours of fasting, the liver generates glucose from pyruvate via gluconeogenesis (GNG). Lactate and alanine feed pyruvate production, and pyruvate is imported into the mitochondrion, where it is preferentially converted into oxaloacetate by pyruvate carboxylase. Oxaloacetate is converted to malate for export back out of the mitochondrion to the cytosol, where it fuels phosphoenol pyruvate (PEP) synthesis and gluconeogenesis (GNG). To determine if BNip3 null liver was defective for GNG in response to fasting, as suggested by reduced hepatic glucose output, we performed a pyruvate challenge in which fasted mice were injected with 1.5 g/kg of sodium pyruvate as an alternative carbon source. BNip3 null mice showed a markedly reduced ability to utilize pyruvate to generate serum glucose in response to fasting compared to results for wild-type mice (Fig. 5A). Similarly, BNip3 null mice were unable to efficiently utilize alanine to promote hepatic glucose production (Fig. 5B), as indicated by lower serum glucose in fasted BNip3 null mice injected with 1.0 g/kg L-alanine.

When we examined expression of key gluconeogenic enzymes, we observed reduced expression of phosphoenolpyruvate carboxykinase (Pepck) and fructose bisphosphatase-1 (Fbp-1) in the BNip3 null liver compared to that in wild-type liver under fed conditions (Fig. 5C and D), consistent with an elevated energy state in BNip3 null liver from fed mice, while expression of the glycolytic enzyme, liver pyruvate kinase (Pklr), was not affected by loss of BNip3 (Fig. 5E). However, these genes were properly induced in BNip3 null liver in response to overnight fasting, suggesting that the reduced hepatic glucose output is not due to inadequate induction of enzymes required for gluconeogenesis. Additionally, these data provide further evidence that loss of BNip3 is not affecting the ability of the liver to receive fasting signals but rather is limiting its ability to respond.

The observed failure of BNip3 null mice to utilize pyruvate or alanine to drive GNG combined with the localization of BNip3 to the outer mitochondrial membrane suggested to us that the defect in hepatic glucose output could be due to defects in shuttling GNG precursors through the mitochondrion. To test this, we first compared the abilities of wild-type versus BNip3 null hepatocytes to utilize either lactate or glycerol to promote glucose output in culture in the presence or absence of forskolin to mimic the fasting signal *in vitro*. Lactate is converted to pyruvate, which must first be shuttled through the mitochondrion in order to fuel GNG, while glycerol inputs GNG upstream of the mitochondrion to provide fructose-bisphosphate and can thus drive hepatic glucose output without the requirement for shuttling intermediates through the mitochondrion. We showed that lactate was not able to restore glucose output by BNip3 null hepatocytes to that observed with wild-type hepatocytes in response to forskolin (Fig. 5F). This is consistent with our previous observation that BNip3 null liver

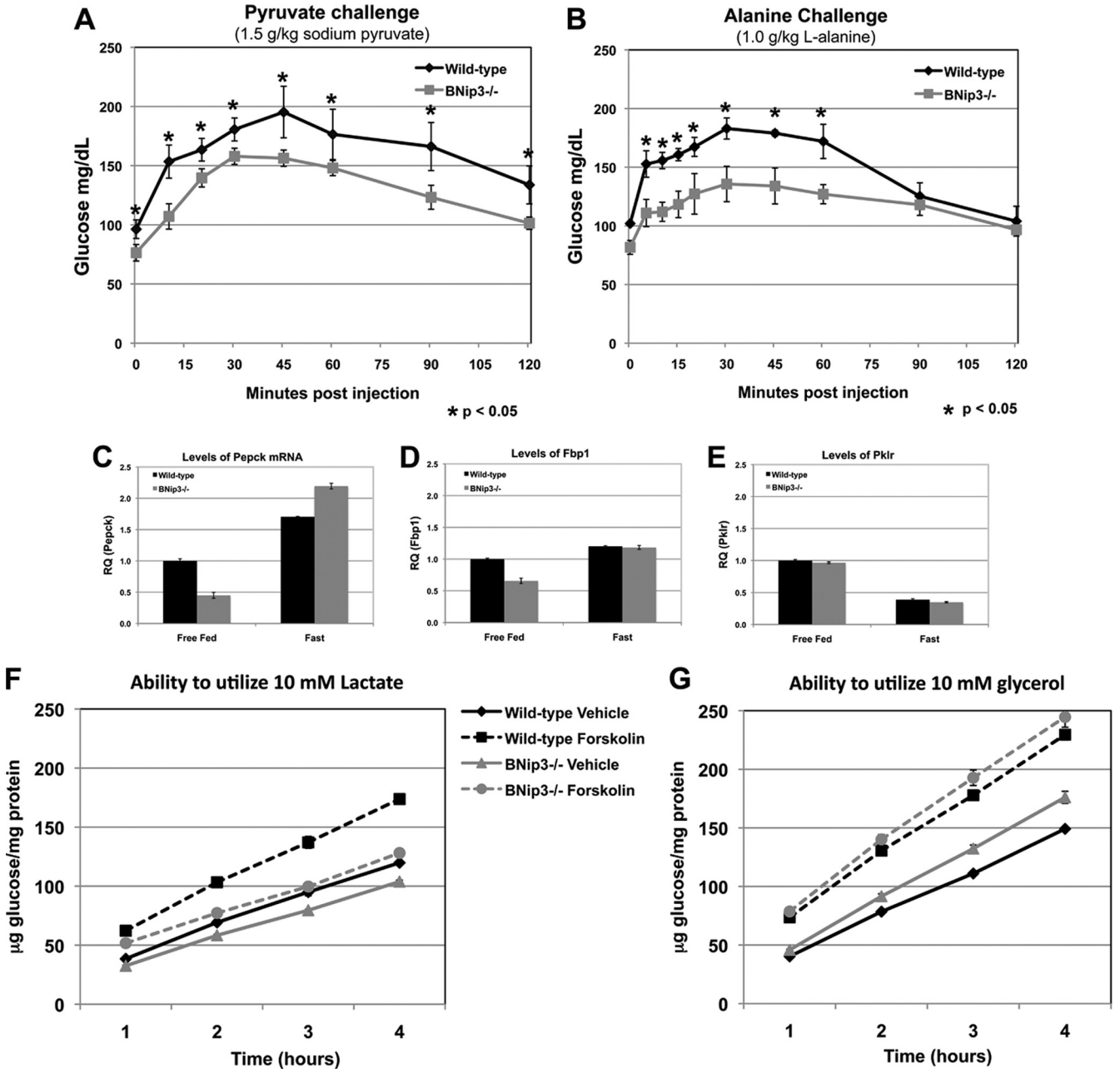

FIG 5 (A) Pyruvate challenge test measuring serum glucose in fasted mice at 15-min intervals after injection with 1.5 g/kg pyruvate ($n = 6$, wild type; $n = 7$, BNip3$^{-/-}$). (B) Alanine challenge measuring serum glucose in fasted mice at 15-min intervals after injection with 1.0 g/kg alanine ($n = 3$, wild type; $n = 3$, BNip3$^{-/-}$). (C to E) Quantitative PCR performed by TaqMan for phosphoenol pyruvate carboxykinase (Pepck), fructose-bisphosphatase-1 (Fbp1), and liver pyruvate kinase (Pklr). (F) Glucose output in culture by wild-type or BNip3 null hepatocytes as a proportion of total protein using [^{13}C]lactate as a carbon source ($n = 6$ for each data set). (G) Glucose output in culture by wild-type or BNip3 null hepatocytes as a proportion of total protein using [^{13}C]glycerol as a carbon source ($n = 6$ for each data set). Data are represented as means + SEM. An unpaired Student *t* test was used for evaluation of statistical significance. The asterisk indicates $P < 0.05$.

cannot efficiently utilize either pyruvate or alanine to increase hepatic glucose production *in vivo* (Fig. 5A and B). In contrast, glycerol was used as effectively by BNip3 null hepatocytes as by wild-type hepatocytes to drive glucose output, which also confirms that there is not a defect at the level of glucose export from the BNip3 null hepatocytes (Fig. 5G). Our results show that there is a reduced capacity for GNG in BNip3 null liver compared to that for the wild type, which likely explains reduced hepatic glucose output in BNip3 null mice under fasting conditions. Furthermore, these data indicate that this defect occurs at the level of the mitochondria, since glycerol but not lactate, alanine, or pyruvate can restore glucose production to wild-type levels.

Increased mitochondrial mass but reduced mitochondrial function in BNip3 null liver. Given the reported role of BNip3 in mitophagy (35, 53, 65, 73) and the importance of functional mitochondria for both lipid metabolism and GNG (11, 38, 40, 47),

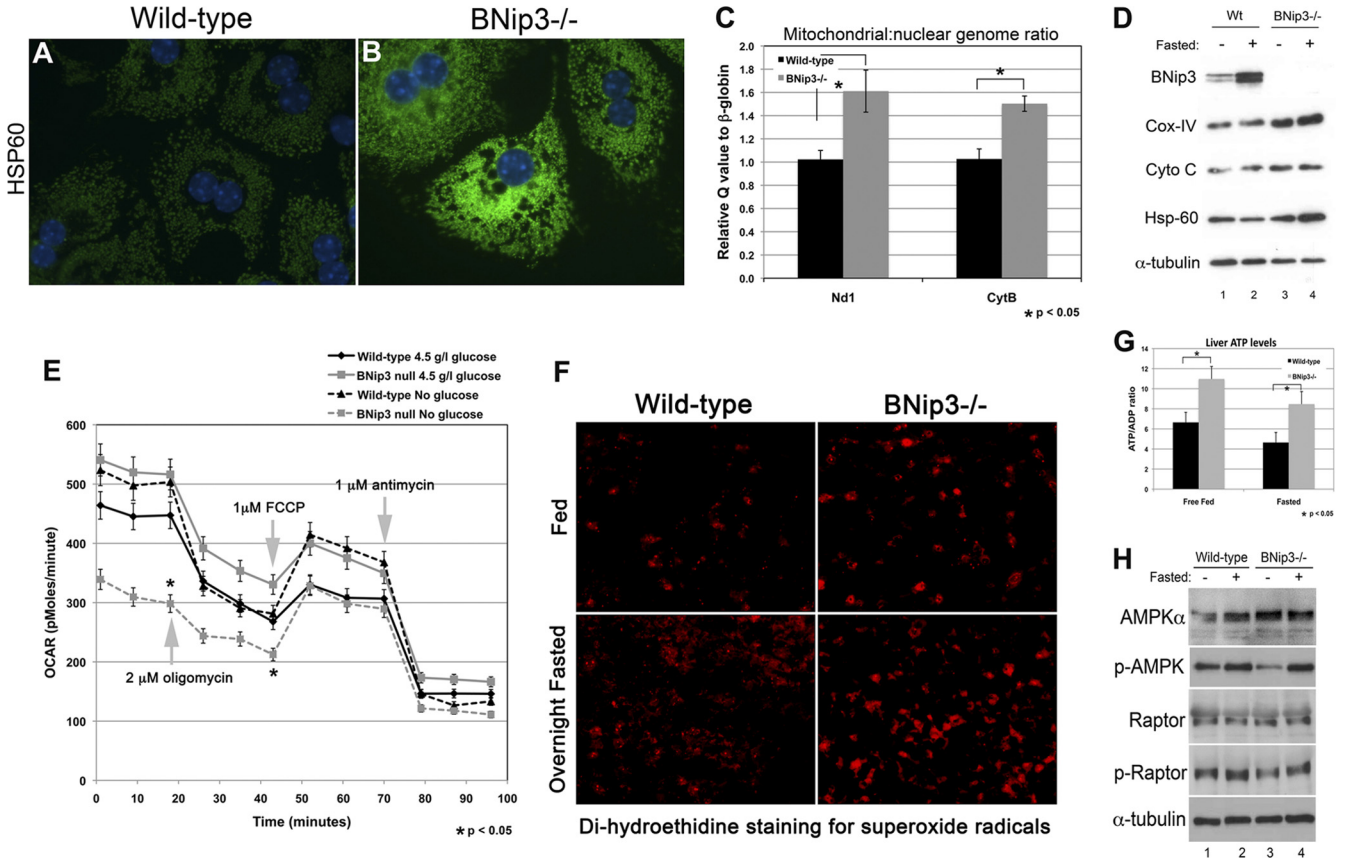

FIG 6 (A and B) Immunofluorescence staining for Hsp60, a mitochondrial matrix protein, on cultured primary hepatocytes isolated from wild-type (A) or BNip3 null (B) mice. (C) Quantitative PCR performed by TaqMan for mitochondrial genome-encoded Nd-1 or cytochrome *b* expressed relative to the amount of nucleus-encoded β-globin on total genomic DNA extracted from wild-type ($n = 9$) and BNip3 null ($n = 9$) mice. (D) Western blot analysis for BNip3, Cox-IV, cytochrome *c*, Hsp60, and α-tubulin on whole-cell liver extracts from adult mice that are free fed or fasted (24 h). (E) Seahorse XF24 measurement of oxygen content by whole hepatocytes freshly isolated from wild-type and BNip3 null liver in the presence or absence of 5 mM glucose. (F) *In situ* staining of frozen liver sections with 2 μM dihydroethidine to detect superoxide levels. (G) Measurement of the ATP-to-ADP ratio in fresh liver isolated from wild-type or BNip3 null mice that were either free fed or fasted for 24 h. (H) Western blot analysis for the α-subunit of AMP-regulated kinase (AMPK), phospho-AMP-regulated kinase (phospho-Thr172), Raptor and phospho-Raptor (Ser792), and α-tubulin on whole-cell liver extracts from adult mice that are free fed (lanes 1 and 3) or fasted (lanes 2 and 4). Data are represented as means + SEM. An unpaired Student *t* test was used for evaluation of statistical significance. The asterisk indicates $P < 0.05$.

we postulated that defective mitophagy could explain the observed metabolic defects in the BNip3 null liver. We performed immunofluorescent staining of primary hepatocyte cultures and observed markedly higher expression of the mitochondrial matrix protein, Hsp60, in BNip3 null hepatocytes (Fig. 6B) than in the wild type (Fig. 6A). Additionally, measurement of mitochondrial genome copy number relative to nuclear genome by quantitative PCR (qPCR) quantified a significant increase in mitochondrial genome number in BNip3 null liver compared to that in wild-type liver (Fig. 6C). Finally, Western blotting confirmed a consistent increase in levels of mitochondrial proteins (Hsp60, Cox-IV, and cytochrome *c*) in BNip3 null liver over those in wild-type liver in both fed and fasted samples (Fig. 6D). These results support the conclusion that loss of BNip3 leads to an increase in mitochondrial mass in BNip3 null liver.

When we measured the respiration of primary hepatocytes in the presence of 5 mM glucose, we observed increased oxygen consumption by BNip3 null hepatocytes compared to that by wild-type hepatocytes (Fig. 6E, solid lines), as might be expected in cells with increased mitochondrial mass. Intriguingly, when we deprived hepatocyte cultures of glucose (Fig. 6E, hashed lines), we observed a dramatic drop-off in respiration by BNip3 null hepatocytes, while wild-type hepatocytes actually increased their respiration, consistent with oxidation of fatty acids, a more efficient energy source than glucose. These observations support the conclusion that while BNip3 null hepatocytes can oxidize glucose more efficiently than wild-type hepatocytes, possibly due to increased mitochondrial mass and increased glycolysis, they are defective at oxidizing alternative carbon sources, such as fatty acids, consistent with data described for Fig. 2E and 2F, identifying a defect in β-oxidation in BNip3 null hepatocytes.

Increased respiration by BNip3 null hepatocytes was also associated with increased generation of superoxide radicals as determined by *in situ* staining for dihydroethidine (DHE), an effect that was exacerbated by overnight fasting (Fig. 6F). Thus, BNip3 loss promotes increased mitochondrial mass and increased respiration but is also associated with elevated production of reactive oxygen species (ROS).

To determine whether the increased respiration rate of BNip3 null hepatocytes promoted increased ATP production, we mea-

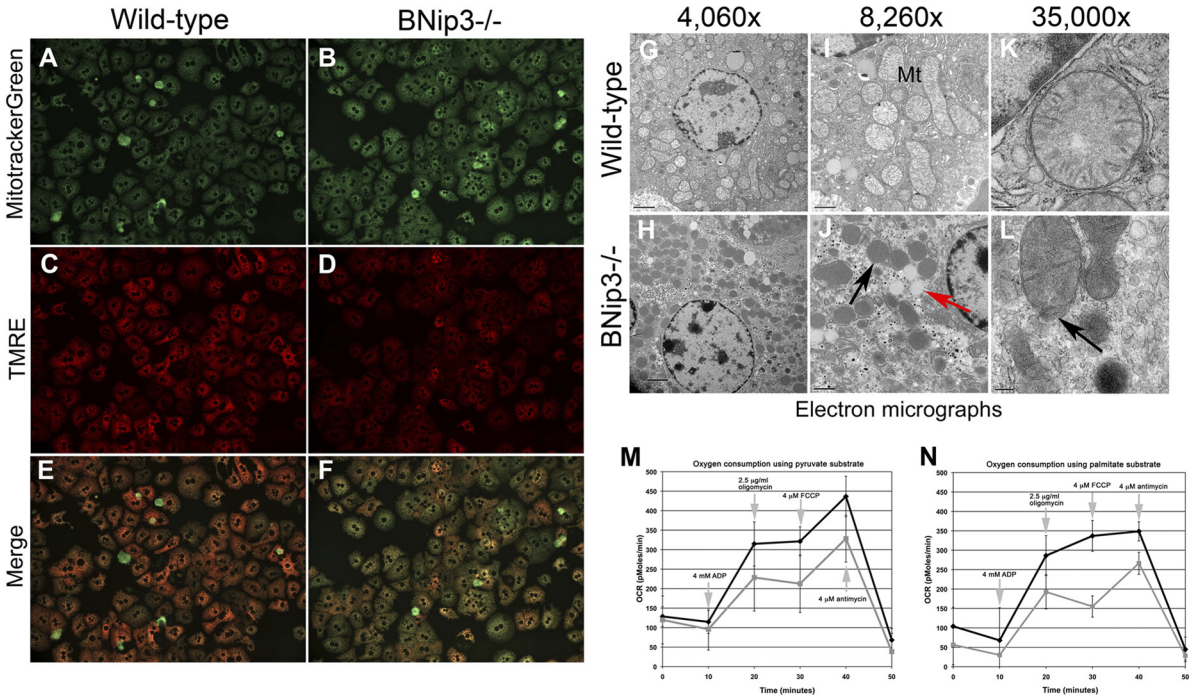

FIG 7 (A to F) Fluorescence microscopy of primary wild-type (A, C, and E) or BNip3 null (B, D, and F) hepatocytes stained with MitoTracker green (A and B) to stain all mitochondria and TMRE (red) as a measure of intact mitochondrial membrane potential (C and D), with the merged images of MitoTracker green and TMRE shown below (E and F). (G to L) Transmission electron microscopy of thin sections from adult mouse liver from wild-type (G, I, and K) or BNip3 null (H, J, and L) mice at increasing magnification. Scale bars are shown in the bottom left of each panel. (M and N) Oxygen consumption by isolated mitochondria from wild-type (red) or BNip3 null (blue) hepatocytes in the presence of 4 mM ADP, 2.5 μg/ml oligomycin, 4 μM FCCP, or 4 μM antimycin using either pyruvate (M) or palmitate (N) as a substrate. Experiments were performed in quadruplicate using the Seahorse Bioscience XF24 machine.

sured ATP and ADP levels in lysates from wild-type and BNip3 null liver collected from free-fed and fasted mice and quantified a significant increase in the ATP/ADP ratio in BNip3 null liver compared to that for the wild type under free-fed conditions (Fig. 6G). High ATP levels and low AMP levels reduce the activity of AMP-regulated kinase (AMPK) (23), and consistent with observed increases in ATP levels, we observed reduced expression of phospho-Thr172-AMPK in liver from free-fed BNip3 null mice compared to wild-type expression (Fig. 6H, lane 3), although overall levels of AMPK subunit α were not changed, indicating reduced activity of AMPK in BNip3 null liver from free-fed mice. Consistently, levels of phospho-Raptor (Ser 792), an established AMPK substrate (21), were also reduced in BNip3 null liver from fed mice (Fig. 6H, lane 3). The observed reduction in AMPK activity in BNip3 null liver may contribute to the observed changes in expression of lipid synthesis enzymes, such as Fasn, Acc, Acly, and Me, that are indirectly suppressed by AMPK activity (37). Overall, our findings that loss of BNip3 leads to increased mitochondrial mass and increased respiration and ATP generation but reduced AMPK activity are consistent with the aberrant sensing of a high-energy state in BNip3 null liver, which in turn results in increased lipogenesis and reduced β-oxidation (Fig. 2), as well as reduced expression of gluconeogenic enzymes under fed conditions (Fig. 5).

While defects in mitophagy increase mitochondrial mass, they also can lead to the accumulation of defective mitochondria (27, 29, 65, 70), and thus we postulated that the inability of BNip3 null mitochondria to oxidize fatty acids properly (Fig. 2) or to efficiently shuttle GNG intermediates to the cytosol (Fig. 5) reflected defective mitochondrial function. Fluorescent staining of live hepatocytes for MitoTracker green (taken up by functional and nonfunctional mitochondria alike) showed increased dye uptake by BNip3 hepatocytes (Fig. 7B) compared to wild-type results (Fig. 7A), confirming that BNip3 null hepatocytes have increased numbers of mitochondria. However, when these primary hepatocyte cultures were stained for TMRE (a potentiometric dye taken up only by functional mitochondria), we observed a marked reduction in TMRE staining in BNip3 null hepatocytes (Fig. 7D) compared to wild-type levels (Fig. 7C), which was most apparent in the merged green-red image (compare Fig. 7F to Fig. 7E). These results indicate that excess mitochondria were accumulating in BNip3 null hepatocytes with a partial loss of membrane potential. When we examined ultrastructural features of liver mitochondria by transmission electron microscopy (TEM) (Fig. 7G to L), we again observed increased numbers of mitochondria in the BNip3 null livers (Fig. 7H) compared to wild-type livers (Fig. 7G), but these excess mitochondria were abnormally small and more electron dense (perhaps reflecting increased long-chain fatty acids) and frequently showed a loss of outer membrane integrity (Fig. 7L, black arrows). TEM also detected increased lipid vesicle content in BNip3 null liver (Fig. 7J, red arrow), consistent with oil red O staining (Fig. 1F). These results support a role for BNip3 in maintaining mitochondrial integrity in adult mouse liver. The observed mitochondrial abnormalities were not associated with an obvious defect in global autophagy, since we observed similar levels of LC3B processing by Western blotting in BNip3 null liver compared to wild-type results (Fig. 8), in contrast to that reported in autophagy-defective Atg7-deficient liver (31). In addition, we did

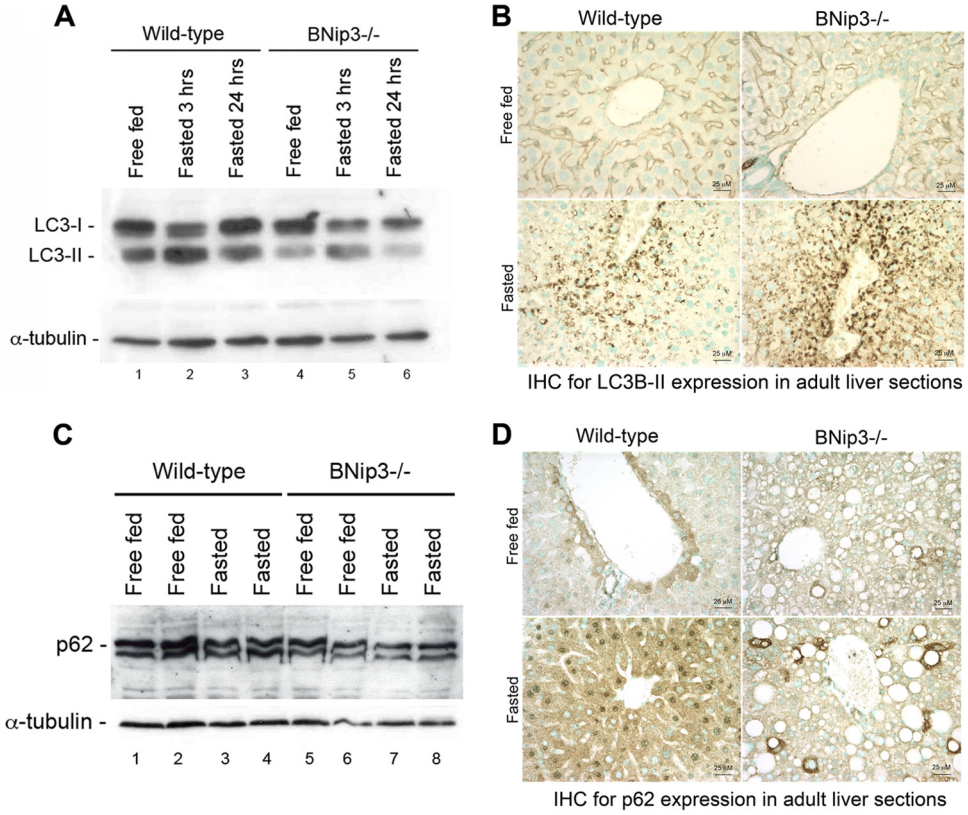

FIG 8 (A) Western blot for LC3B on whole-cell liver extracts from wild-type and BNip3 null mice that were fasted for 0, 3, or 24 h. (B) Immunohistochemical staining for the autophagy marker, processed LC3B-II, on wild-type and BNip3 null liver before and after fasting. (C) Western blot analysis of p62/sequestrin on whole-cell liver extracts from wild-type and BNip3 null mice that were fasted for 0 or 24 h. (D) Immunohistochemical staining for p62/sequestrin on wild-type and BNip3 null liver before and after fasting.

not observe an accumulation of p62 in BNip3 null liver (Fig. 8C), as would be expected if there was a more general defect in autophagy (30, 31). Interestingly, immunohistochemical staining revealed differences in the zonal patterning of both LC3B-II and p62 in wild-type liver, with increased perivenous staining and reduced periportal staining in wild-type liver in response to 24 h of fasting (Fig. 8B and D). In the BNip3 null liver, this increase in punctate LC3B-II in perivenous regions of the liver was more marked, confirming that the response to fasting was intact and suggesting that defective mitochondria may actually increase levels of autophagy in regions of the liver, possibly due to the observed insufficiencies in β-oxidation. While overall p62 did not accumulate in BNip3 null liver, we observed localized increases in p62 in individual hepatocytes (Fig. 8D), suggesting that some cells in the BNip3 liver were defective for autophagy, possibly due to the marked accumulation of lipid.

Although BNip3 null hepatocytes isolated from 3-month-old male mice showed an overall increase in respiration when cultured in 5 mM glucose (Fig. 6E), this could be attributed to the overall increase in mitochondrial mass in BNip3 null mice (Fig. 6B to D). When we performed respiration studies with isolated mitochondria using pyruvate as a substrate for oxidation, we observed that mitochondria from BNip3 null liver consumed less oxygen in the presence of ADP (added after 10 min) than an equal number of wild-type control mitochondria (Fig. 7M). This effect was particularly marked when the ATPase proton pump was inhibited at 20 min with oligomycin (Fig. 7M). The failure to maintain oxygen consumption when oligomycin was added indicates that healthy mitochondria isolated from BNip3 null liver are more dependent on oxidative phosphorylation for ATP generation than wild-type mitochondria. This effect was particularly striking when palmitate rather than pyruvate was used as a substrate (Fig. 7N), consistent with BNip3 null mitochondria being defective for fatty acid oxidation, as determined above in other assays (Fig. 2E and 6E). These results show that loss of BNip3 leads to increased mitochondrial mass with a concomitant increase in mitochondrial dysfunction.

BNip3 null mice develop steatohepatitis. In addition to increased lipid accumulation (Fig. 1 and 2) and elevated reactive oxygen species accumulation (Fig. 6H), histological analysis revealed increased leukocyte infiltration into the liver of BNip3 null mice (Fig. 9B, black arrows) compared to findings for wild-type liver (Fig. 9A). These inflammatory infiltrates included neutrophils that stained positively for myeloperoxidase (Fig. 9C) and B lymphocytes that stained positively for B220 (Fig. 9D). The proximity of leukocyte infiltration (Fig. 9F, black arrow) to regions of the BNip3 liver that stained positive by TUNEL assay (Fig. 9F, red arrows) suggested that the increased inflammation was linked to cell death of hepatocytes. Indeed, PAS staining identified PAS-positive hepatocyte remnants (Fig. 9G and H, white arrows) inside resident tissue phagocytes (dark-staining nuclei) under both free-

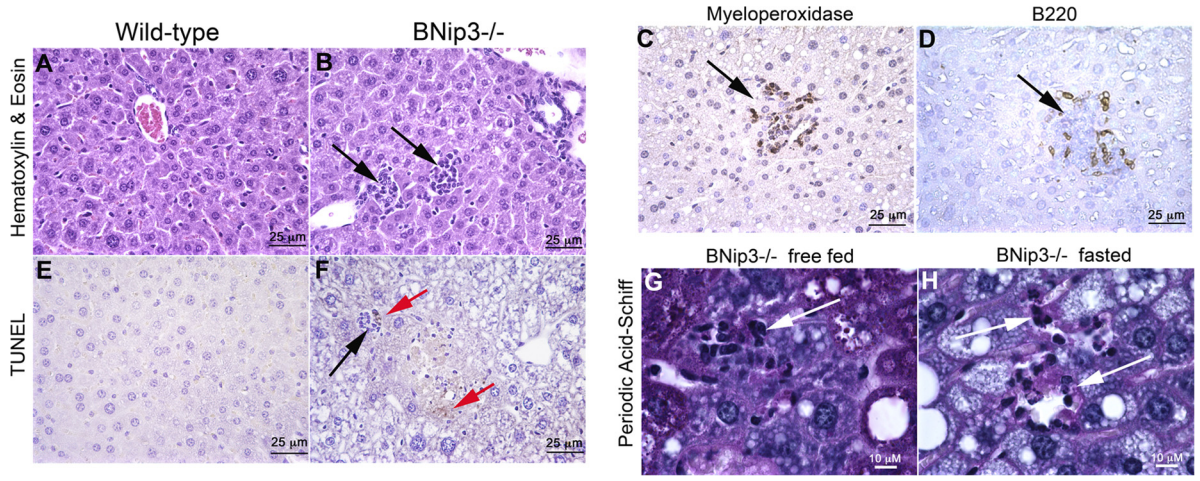

FIG 9 (A and B) Hematoxylin-and-eosin staining of wild-type (A) or BNip3 null (B) liver (black arrows indicate infiltrating leukocytes). (C) Immunohistochemical staining for the neutrophil-specific marker myeloperoxidase on BNip3 null liver. (D) Immunohistochemical staining for the B cell-specific marker B220 on BNip3 null liver. (E and F) TUNEL staining of wild-type (E) or BNip3 null (F) liver. Black arrows indicate infiltrating leukocytes. Red arrows indicate regions staining positive for TUNEL. (G and H) PAS staining of liver from free-fed and 24-h-fasted BNip3 null livers at magnification ×1,000, highlighting regions of cell death in which PAS-positive hepatocellular cytoplasm is detected in resident phagocytes (white arrows).

fed and fasted conditions, indicating that loss of BNip3 leads to steatohepatitis.

In summary, we have identified a key role for BNip3 in the liver to limit lipogenesis and promote fatty acid oxidation in the fed state and promote gluconeogenesis in the fasted state. Specifically, we propose that by limiting mitochondrial mass and promoting mitochondrial integrity, BNip3 is required in the liver to regulate energy homeostasis, with a loss of BNip3 leading to increased mitochondrial mass, elevated ATP, and reduced AMPK activity, resulting in the aberrant sensing of a high-energy state in the liver. However, increased mitochondrial mass was offset by reduced mitochondrial function and was associated with increased reactive oxygen species generation, inflammation, and steatohepatitis. This work demonstrates how a loss of BNip3 results in altered metabolic states and reduced mitochondrial integrity and highlights the importance of examining mitophagy in diseases linked to irregular lipid and glucose maintenance.

DISCUSSION

The liver integrates systemic control of glucose output to the blood in response to nutrient availability (38). Imbalances between anabolic processes in the liver, such as lipid synthesis under fed conditions and catabolic processes, such as β-oxidation of fatty acids and gluconeogenesis in response to fasting, have been implicated in liver diseases, such as nonalcoholic fatty liver disease (NAFLD) and nonalcoholic steatohepatitis (NASH), as well as hepatic insulin resistance and type 2 diabetes (5, 38, 43, 47, 61). Given that the mitochondrion is the major site of fatty acid oxidation, Krebs cycle, and oxidative phosphorylation in the cell, there is considerable interest in explaining how altered mitochondrial function contributes to the pathobiology of metabolic diseases (2, 11, 36, 40, 47, 48, 61). To date, such mitochondrial defects include abnormalities in fatty acid oxidation (12, 33, 63, 72), mitochondrial biogenesis (66, 69), and oxidative phosphorylation (2, 10, 50). Our data demonstrate for the first time a specific role for mitophagy in maintaining liver homeostasis.

Increased mitochondrial mass in BNip3 null liver is offset by reduced mitochondrial function. Mitophagy is a key cellular process used to eliminate dysfunctional mitochondria (62, 70), and indeed, De Duve's observation that glucagon induced mitochondrial autophagy in the liver was the basis of his Nobel prize awarded in 1974 (13, 14). We have identified a novel role for BNip3 in regulating the balance between lipid synthesis and fatty acid oxidation in the liver and in promoting gluconeogenesis in response to fasting. Consistent with this role, BNip3 is induced in the liver in response to fasting, and loss of BNip3 increased insulin sensitivity while reducing glucagon responsiveness. We suggest that this phenotype is consistent with the canonical function of BNip3 as a regulator of mitochondrial fragmentation and mitophagy (35, 53, 65, 73), given that increased mitochondrial mass is observed in BNip3 null liver as expected if mitochondrial turnover is reduced (Fig. 10A). However, increased mitochondrial mass was offset by reduced mitochondrial function in terms of structural integrity, membrane polarization, and oxygen consumption (Fig. 10B).

These two consequences of BNip3 loss undoubtedly oppose each other in terms of effect on ATP production at the mitochondria, with increased mitochondrial mass promoting increased oxygen consumption and ATP generation (Fig. 10B) while reduced mitochondrial function leads to reduced β-oxidation, mitochondrial overload, reduced oxygen consumption, reduced ATP production, and ROS production (Fig. 10B and C). The net effect on ATP levels will therefore likely be the balance of these two opposing effects of BNip3 loss—in other words, determined by how many of the surplus mitochondria are functional. Our results show that the ATP/ADP ratio is increased in BNip3 null liver from free-fed mice at 3 months of age compared to results for age-matched wild-type mice, suggesting that the positive effects of increased mitochondrial mass on ATP production initially predominate over the negative effect of reduced mitochondrial function (Fig. 10C). However, we predict that this balance will shift with increasing age of the mice, and ongoing work is aimed at addressing this intriguing issue.

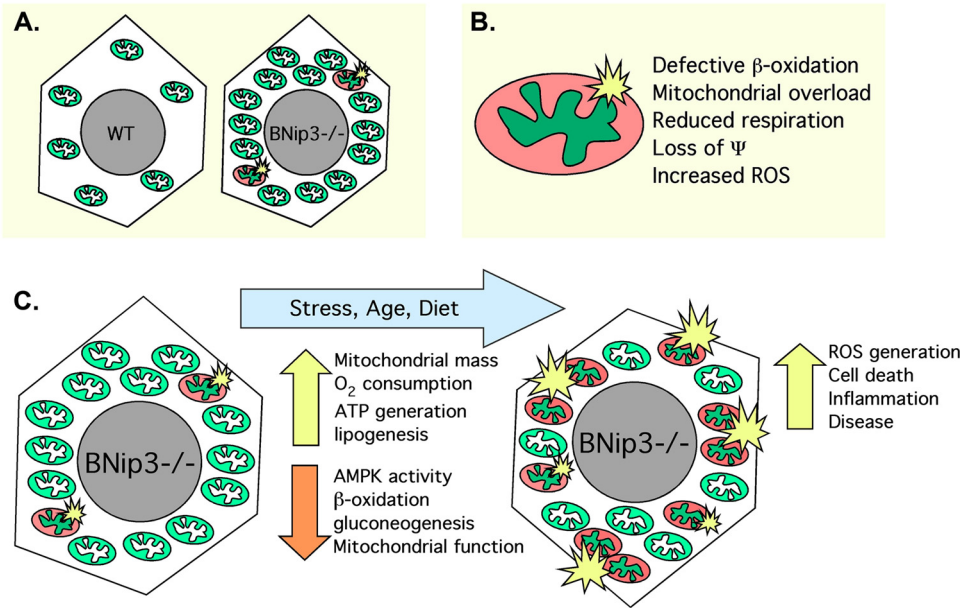

FIG 10 (A) Loss of BNip3 leads to increased mitochondrial mass in the liver due to a defect in turnover of mitochondria at the autophagosome (mitophagy). Increased mitochondrial mass leads to increased oxygen consumption, increased ATP production, and the aberrant sensing of a high-energy state, leading to increased lipogenesis. (B) Failure to turn over mitochondria leads to increased mitochondrial mass but the accumulation of defective mitochondria that are unable to carry out β-oxidation of fatty acids properly and accumulation of long-chain fatty acids in the mitochondria, further exacerbating mitochondrial dysfunction, resulting in a loss of membrane potential and ROS production. (C) The effect of BNip3 on liver metabolism is therefore likely to be determined by the balance between levels of mitochondria and the proportion that are functional for β-oxidation of fatty acids, oxidative phosphorylation, and gluconeogenesis. Over time, in the absence of increased biogenesis or cell proliferation, the balance will move toward increased mitochondrial dysfunction, which can lead to cell death, compensating proliferation, inflammation, and disease.

Aberrant sensing of a high-energy state is associated with increased mitochondrial mass, increased respiration, and elevated ATP production. Our work shows that elevated ATP production resulting from increased mitochondrial mass in BNip3 null liver leads to the aberrant sensing of a high-energy state, as confirmed by reduced AMPK activity (Fig. 6H), increased expression of lipogenic enzymes, and increased lipid synthesis (Fig. 2). Reduced AMPK activity blocks β-oxidation of fatty acids and increases lipogenesis (24), both features of altered metabolism observed in BNip3 null liver. Of note, the lipogenic enzymes that we show to be induced in BNip3 null liver (Fasn, Acc, Acly, and Me) are all transcriptionally regulated by SREBP1 (11), which is in turn inhibited by AMPK-dependent phosphorylation (37). Increased Acc may also explain reduced transport of fatty acids into the mitochondria, reduced β-oxidation of fatty acids under fed conditions (Fig. 2) modulated through Acc2 activity at the outer mitochondrial membrane, and increased lipogenesis through increased AccI activity in the cytosol. In summary, our work indicates that reduced mitophagy leads to steatosis in the liver and predicts that activating AMPK should limit lipogenesis in the BNip3 null liver; however, AMPK activation would not necessarily rescue other effects of mitochondrial dysfunction on the metabolic phenotype observed in BNip3 null mice, such as reduced β-oxidation of fatty acids or reduced gluconeogenesis.

Defective β-oxidation of fatty acids in BNip3 null hepatocytes. Our work here has identified for the first time a role for BNip3 in regulating mitochondrial mass and integrity in the liver that has significance for liver metabolism and disease. Loss of mitochondrial function may be the result of increased ROS produced at the mitochondria that damages lipid membranes or protein function, which then results in defective β-oxidation and gluconeogenesis. Conversely, the defect in β-oxidation may be damaging mitochondria as long-chain fatty acids accumulate in the matrix, resulting in mitochondrial overload, and this may be the major causative factor that limits gluconeogenesis and feeds back to further inhibit fatty acid oxidation. For example, intramitochondrial accumulation of acyl-CoAs induced by high-fat feeding of mice resulted in hepatic insulin resistance that corresponded directly with the degree of mitochondrial dysfunction, including reduced respiration and reduced fatty acid oxidation (33, 47).

This cause-and-effect dilemma posed by our data raises the possibility that BNip3 plays additional, more direct roles in metabolism over and above its function in mitophagy. For example, BNip3 has been reported to interact directly with acetyl-CoA acyl transferase 2 (Acaa2), an enzyme involved in fatty acid oxidation in the mitochondrial matrix (6). However, BNip3 localizes to the outer mitochondrial membrane, making an interaction with a matrix protein such as Acaa2 unlikely. In contrast, Acc2 does colocalize with BNip3 to the outer mitochondrial membrane and is negatively regulated by AMPK (23, 58). Together with our data showing upregulation of Acc2 in BNip3 null liver and the key role of Acc2 downstream of AMPK activity in inhibiting β-oxidation through inhibition of Cpt-1 activity, this suggests that perhaps Acc2 is negatively regulated by BNip3 at the outer mitochondrial membrane. Given that loss of Acc2 in mice protects against obesity and diabetes induced by a high-fat diet by increasing uptake of fatty acid by mitochondria and promoting β-oxidation of fatty acids (1), it may therefore be useful to examine how overexpression (as opposed to loss) of BNip3 affects hepatic insulin resistance and other aspects of metabolic disease.

BNip3 as a downstream mediator of Hif effects on liver metabolism. BNip3 is a HIF target gene, and regional hypoxia plays an important role in gene regulation and zonation of metabolic activities in the liver (26). We observed increased BNip3 protein levels in liver that is deleted for Hif-2α (Fig. 1B), suggesting that Hif-2α may repress BNip3 expression in liver. Intriguingly, liver-specific deletion of the Von Hippel-Lindau (*Vhl*) tumor suppressor in mice resulted in hepatic steatosis and hypoglycemia (51), an effect that was specifically dependent on Hif-2α, such that knockout of Hif-2α but not Hif-1α rescued the observed steatosis and hypoglycemia. Thus, it will be interesting to determine the extent to which rescue of the phenotype in *Vhl*-deleted liver by Hif-2α deletion is dependent on derepression of BNip3. It will also be interesting to determine the mechanism by which BNip3 is induced by fasting signals and how these signals are integrated into liver homeostatic responses to changing systemic nutrient supply.

In summary, our work has revealed a novel connection between defective mitophagy and regulation of lipid metabolism in the liver that has ramifications for the etiology of diseases linked to hepatic steatosis, such as NASH and type 2 diabetes. This work identifies BNip3 as a potential target for therapeutic intervention if the mechanisms regulating its levels and activity in liver can be elucidated.

ACKNOWLEDGMENTS

Work on this project was supported by a University of Chicago Digestive Disease Research Core Center grant (P30 DK42086), The University of Chicago Diabetes Research and Training Center Pilot and Feasibility Grant Program (P60 DK-20595), and NIH grant RO1 CA131188 (to K.F.M.).

We thank Marina Sharifi and Lauren Olson for critical reading of the manuscript. We also thank Chris Rhodes and his laboratory for advice during the course of this work. We thank Yimei Chen and Terri Li for expert technical support in electron microscopy and tissue sectioning, respectively.

REFERENCES

1. **Abu-Elheiga L, Oh W, Kordari P, Wakil SJ.** 2003. Acetyl-CoA carboxylase 2 mutant mice are protected against obesity and diabetes induced by high-fat/high carbohydrate diets. Proc. Natl. Acad. Sci. U. S. A. **100**: 10207–10212.
2. **Begriche K, Igoudjil A, Pessayre D, Fromenty B.** 2006. Mitochondrial dysfunction in NASH: causes, consequences and possible means to prevent it. Mitochondrion **6**:1–28.
3. **Bellot G, et al.** 2009. Hypoxia-induced autophagy is mediated through HIF-induction of BNIP3 and BNIP3L via their BH3 domains. Mol. Cell. Biol. **29**:2570–2581.
4. **Bruick RK.** 2000. Expression of the gene encoding the proapoptotic Nip3 protein is induced by hypoxia. Proc. Natl. Acad. Sci. U. S. A. **97**:9082–9087.
5. **Brunt EM.** 2004. Nonalcoholic steatohepatitis. Semin. Liver Dis. **24**:3–20.
6. **Cao W, et al.** 2008. Acetyl-coenzyme A acyltransferase 2 attenuates the apoptotic effects of BNIP3 in two human cell lines. Biochim. Biophys. Acta **1780**:873–880.
7. **Chen G, et al.** 1999. Nix and Nip3 form a subfamily of pro-apoptotic mitochondrial proteins. J. Biol. Chem. **274**:7–10.
8. **Chen G, et al.** 1997. The E1B 19K/Bcl2 binding protein Nip3 is a dimeric mitochondrial protein that activates apoptosis. J. Exp. Med. **186**:1975–1983.
9. **Chen Y, et al.** 2010. Dual autonomous mitochondrial cell death pathways are activated by Nix/BNip3L and induce cardiomyopathy. Proc. Natl. Acad. Sci. U. S. A. **107**:9035–9042.
10. **Cheng Z, et al.** 2009. Foxo1 integrates insulin signaling with mitochondrial function in the liver. Nat. Med. **15**:1307–1311.
11. **Cheng Z, Tseng Y, White MF.** 2010. Insulin signaling meets mitochondria in metabolism. Trends Endocrinol. Metab. **21**:589–598.
12. **Choi CS, et al.** 2007. Continuous fat oxidation in acetyl-CoA carboxylase 2 knockout mice increases total energy expenditure, reduces fat mass and improves insulin sensitivity. Proc. Natl. Acad. Sci. U. S. A. **104**:16480–16485.
13. **Deter RL, Baudhuin P, De Duve C.** 1967. Participation of lysosomes in cellular autophagy induced in rat liver by glucagon. J. Cell Biol. **35**:C11–C16.
14. **Deter RL, De Duve C.** 1967. Influence of glucagon, an inducer of cellular autophagy, on some physical properties of rat liver lysosomes. J. Cell Biol. **33**:437–449.
15. **Diwan A, et al.** 2007. Inhibition of ischemic cardiomyocyte apoptosis through targeted ablation of BNip3 restrains postinfarction remodeling in mice. J. Clin. Invest. **117**:2825–2833.
16. **Diwan A, et al.** 2009. Endo-plasmic reticulum-mitochondria crosstalk in NIX-mediated murine cell death. J. Clin. Invest. **119**:203–212.
17. **Dominy JE, Lee YS, Gerhart-Hines Z, Puigserver P.** 2010. Nutrient-dependent regulation of PGC-1a's acetylation state and metabolic function through the enzymatic activities of Sirt1/GCN5. Biochim. Biophys. Acta **1804**:1676–1683.
18. **Dorn GW, II.** 2010. Mitochondrial pruning by NIX and BNIP3: an essential function for cardiac-expressed death factors. J. Cardiovasc. **3**:374–383.
19. **Ezaki J, et al.** 2011. Liver autophagy contributes to the maintenance of blood glucose and amino acid levels. Autophagy **7**:727–736.
20. **Gruber M, et al.** 2007. Acute post-natal ablation of Hif-2a results in anemia. Proc. Natl. Acad. Sci. U. S. A. **104**:2301–2306.
21. **Gwinn DM, et al.** 2008. AMPK phosphorylation of raptor mediates a metabolic checkpoint. Mol. Cell **30**:214–226.
22. **Hamacher-Brady A, et al.** 2007. Response to myocardial ischemia/reperfusion injury involves BNip3 and autophagy. Cell Death Differ. **14**: 146–157.
23. **Hardie DG.** 2011. AMP-activated protein kinase—an energy sensor that regulates all aspects of cell function. Genes Dev. **25**:1895–1908.
24. **Hardie DG.** 2011. Energy sensing by the AMP-activated protein kinase and its effects on muscle metabolism. Proc. Nutr. Soc. **70**:92–99.
25. **Jin S.** 2006. Autophagy, mitochondrial quality control and oncogenesis. Autophagy **2**:80–84.
26. **Jungermann K, Kietzmann T.** 2000. Oxygen: modulator of metabolic zonation and disease of the liver. Hepatology **31**:255–260.
27. **Karantza-Wadsworth V, et al.** 2007. Autophagy mitigates metabolic stress and genome damage in mammary tumorigenesis. Genes Dev. **21**: 1621–1635.
28. **Kim I, Lemasters JJ.** 2011. Mitochondrial degradation by autophagy (mitophagy) in GFP-LC3 transgenic hepatocytes during nutrient deprivation. Am. J. Physiol. Cell Physiol. **300**:C308–C317.
29. **Kim I, Rodriguez-Enriquez S, Lemasters JJ.** 2007. Selective degradation of mitochondria by mitophagy. Arch. Biochem. Biophys. **462**:245–253.
30. **Komatsu M, et al.** 2007. Homeostatic levels of p62 control cytoplasmic inclusion body formation in autophagy-deficient mice. Cell **131**:1149–1163.
31. **Komatsu M, et al.** 2005. Impairment of starvation-induced and constitutive autophagy in Atg7-deficient mice. J. Cell Biol. **169**:425–434.
32. **Koppenol WH, Bounds PL, Dang CV.** 2011. Otto Warburg's contributions to current concepts of cancer metabolism. Nat. Rev. Cancer **11**:325–337.
33. **Koves TR, et al.** 2008. Mitochondrial overload and incomplete fatty acid oxidation contribute to skeletal muscle insulin resistance. Cell Metab. **7**:45–56.
34. **Kubasiak LA, Hernandez OM, Bishopric NH, Webster KA.** 2002. Hypoxia and acidosis activate cardiac myocyte death through the bcl-2 family protein BNIP3. Proc. Natl. Acad. Sci. U. S. A. **99**:12825–12830.
35. **Landes T, et al.** 2010. The BH3-only BNip3 binds to the dynamin Opa1 to promote mitochondrial fragmentation and apoptosis by distinct mechanisms. EMBO Rep. **11**:459–465.
36. **Li LO, et al.** 2009. Liver-specific loss of long chain acyl-CoA synthetase-1 decreases triacylglycerol synthesis an b-oxidation and alters phospholipid fatty acid composition. J. Biol. Chem. **284**:27816–27826.
37. **Li Y, et al.** 2011. AMPK phosphorylates and inhibits SREBP activity to attenuate hepatic steatosis and atherosclerosis in diet-induced insulin-resistant mice. Cell Metab. **13**:376–388.
38. **Lin HV, Accili D.** 2011. Hormonal regulation of hepatic glucose production in health and disease. Cell Metab. **14**:9–19.
39. **Lingohr MK, Bull RJ, Kato-Weinstein J, Thrall BD.** 2002. Dichloroac-

etate stimulates glycogen accumulation in primary hepatocytes through an insulin-independent mechanism. Toxicol. Sci. **68**:508–515.
40. **Lowell BB, Shulman GI.** 2005. Mitochondrial dysfunction and type 2 diabetes. Science **307**:384–387.
41. **Macleod K, Hu Y, Jacks T.** 1996. Loss of Rb activates both p53-dependent and -independent cell death pathways in the developing mouse nervous system. EMBO J. **15**:6178–6188.
42. **Majmundar AJ, Wong WJ, Simon MC.** 2010. Hypoxia-inducible factors and the response to hypoxic stress. Mol. Cell **40**:294–309.
43. **Marchesini G, Marzocchi R, Agostini F, Bugianesi E.** 2005. Nonalcoholic fatty liver disease and the metabolic syndrome. Curr. Opin. Lipidol. **16**:421–427.
44. **Mathew R, et al.** 2009. Autophagy suppresses tumorigenesis through elimination of p62. Cell **137**:1062–1075.
45. **Moon A, Rhead WJ.** 1987. Complementation analysis of fatty acid oxidation disorders. J. Clin. Invest. **79**:59–64.
46. **Muoio DM, Newgard CB.** 2006. Obesity-related derangements in metabolic regulation. Annu. Rev. Biochem. **75**:367–401.
47. **Muoio DM, Newgard CB.** 2008. Molecular and metabolic mechanisms of insulin resistance and β-cell failure in type 2 diabetes. Nat. Rev. Mol. Biol. **9**:193–205.
48. **Noland RC, et al.** 2009. Carnitine insufficiency caused by aging and overnutrition compromises mitochondrial performance and metabolic control. J. Biol. Chem. **284**:22840–22852.
49. **Papandreou I, et al.** 2005. Anoxia is necessary for tumor cell toxicity caused by a low-oxygen environment. Cancer Res. **65**:3171–3178.
50. **Pospisilik JA, et al.** 2007. Targeted deletion of AIF decreases mitochondrial oxidative phosphorylation and protects from obesity and diabetes. Cell **131**:476–491.
51. **Rankin EB, et al.** 2009. Hypoxia-inducible factor 2 regulates hepatic lipid metabolism. Mol. Cell. Biol. **29**:4527–4538.
52. **Ray R, et al.** 2000. BNIP3 heterodimerizes with Bcl-2/Bcl-XL and induces cell death independent of a Bcl-2 homology 3 (BH3) domain at both mitochondrial and nonmitochondrial sites. J. Biol. Chem. **275**:1439–1448.
53. **Rikka S, et al.** 2011. BNip3 impairs mitochondrial bioenergetic and stimulates mitochondrial turnover. Cell Death Differ. **18**:721–731.
54. **Saltiel AR, and KCR.** 2001. Insulin signalling and the regulation of glucose and lipid metabolism. Nature **414**:799–806.
55. **Sandoval H, et al.** 2008. Essential role for Nix in autophagic maturation of red cells. Nature **454**:232–235.
56. **Schwarten M, et al.** 2009. Nix binds to GABARAP: a possible crosstalk between apoptosis and autophagy. Autophagy **5**:690–698.
57. **Schweers RL, et al.** 2007. NIX is required for programmed mitochondrial clearance during reticulocyte maturation. Proc. Natl. Acad. Sci. U. S. A. **104**:19500–19505.
58. **Shackelford DB, Shaw RJ.** 2009. The LKB1-AMPK pathway: metabolism and growth control in tumour suppression. Nat. Rev. Cancer **9**:563–575.
59. **Singh R, et al.** 2009. Autophagy regulates lipid metabolism. Nature **458**:1131–1139.
60. **Syed FM, et al.** 2004. Physiological growth synergizes with pathological genes in experimental cardiomyopathy. Circ. Res. **95**:1200–1206.
61. **Szendroedi J, Phielix E, Roden M. 13 September**2011. The role of mitochondria in insulin resistance and type 2 diabetes mellitus. Nat. Rev. Endocrinol. doi:10.1038/nrendo.2011.138. [Epub ahead of print.]
62. **Tolkovsky AM.** 2009. Mitophagy. Biochim. Biophys. Acta **1793**:1508–1515.
63. **Tolwani RJ, et al.** 2005. Medium chain acyl-CoA dehydrogenase deficiency in gene targeted mice. PLoS Genet. **1**:205–211. doi:10.1371/journal.pgen.0010023.
64. **Tracy K, et al.** 2007. BNIP3 is a RB/E2F target gene required for hypoxia-induced autophagy. Mol. Cell. Biol. **27**:6229–6242.
65. **Tracy K, Macleod KF.** 2007. Regulation of mitochondrial integrity, autophagy and cell survival by BNIP3. Autophagy **3**:616–619.
66. **Vianna CR, et al.** 2006. Hypomorphic mutation of PGC-1b causes mitochondrial dysfunction and liver insulin resistance. Cell Metab. **4**:453–464.
67. **Yang L, Li P, Fu S, Calay ES, Hotamisligil GS.** 2010. Defective hepatic autophagy in obesity promotes ER stress and causes insulin resistance. Cell Metab. **11**:467–478.
68. **Yasuda M, Theodorakis P, Subramanian T, Chinnadurai G.** 1998. Adenovirus E1B-19K/Bcl2 interacting protein BNIP3 contains a BH3 domain and a mitochondrial targeting sequence. J. Biol. Chem. **273**:12415–12421.
69. **Yoon JC, et al.** 2010. Wnt signaling regulates mitochondrial physiology and insulin sensitivity. Genes Dev. **24**:1507–1518.
70. **Youle RJ, Narendra DP.** 2011. Mechanisms of mitophagy. Nat. Rev. Mol. Biol. **12**:9–14.
71. **Zhande R, et al.** 2006. Dephosphorylation by default, a potential mechanism for regulation of insulin receptor substrate-1/2, Akt, and ERK1/2. J. J. Biol. Chem. **281**:39071–39080.
72. **Zhang D, et al.** 2007. Mitochondrial dysfunction due to long-chain Acyl-CoA dehydrogenase deficiency causes hepatic steatosis and hepatic insulin resistance. Proc. Natl. Acad. Sci. U. S. A. **104**:17075–17080.
73. **Zhang H, et al.** 2008. Mitochondrial autophagy is a HIF-1 dependent adaptive metabolic response to hypoxia. J. Biol. Chem. **283**:10892–10903.
74. **Zhang H, et al.** 2007. HIF-1 inhibits mitochondrial biogenesis and cellular respiration in VHL-deficient renal cell carcinoma by repression of c-Myc activity. Cancer Cell **11**:407–420.
75. **Zhang L, Li L, Liu H, Borowitz JL, Isom GE.** 2009. BNIP3 mediates cell death by different pathways following localization to endoplasmic reticulum and mitochondrion. FASEB J. **23**:3405–3414.